Chemical Engineering Journal 283 (2016) 388–396

Contents lists available at ScienceDirect

Chemical Engineering Journal

journal homepage: www.elsevier.com/locate/cej

Lithium orthosilicate for CO_2 capture with high regeneration capacity: Kinetic study and modeling of carbonation and decarbonation reactions

Suélen M. Amorim [a,*], Michele D. Domenico [a], Tirzhá L.P. Dantas [b], Humberto J. José [a], Regina F.P.M. Moreira [a]

[a] Department of Chemical Engineering, Federal University of Santa Catarina, 88040-900 Florianópolis, SC, Brazil
[b] Department of Chemical Engineering, Federal University of Paraná, 80060-000 Curitiba, PR, Brazil

HIGHLIGHTS

- This work presents a kinetic study and modeling of the CO_2 capture of Li_4SiO_4.
- After 48 carbonation/decarbonation cycles the solid showed an activity decay of 20%.
- The shrinking core model was firstly applied to Li_4SiO_4 decarbonation.
- This model adequately described both kinetics of carbonation and decarbonation.

GRAPHICAL ABSTRACT

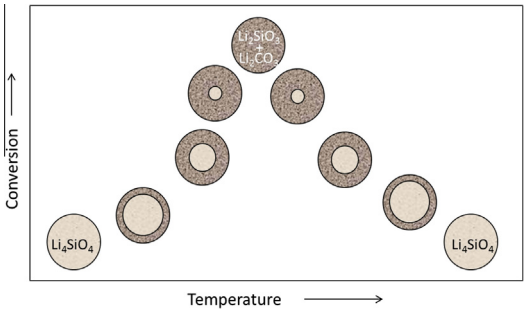

ARTICLE INFO

Article history:
Received 26 May 2015
Received in revised form 25 July 2015
Accepted 27 July 2015
Available online 1 August 2015

Keywords:
Lithium orthosilicate
CO_2 capture
Shrinking core model
Kinetic parameters

ABSTRACT

One of the most promising techniques for CO_2 capture at high temperatures consists in its separation by the carbonation reaction with an inorganic solid. Lithium orthosilicate (Li_4SiO_4) is considered one potential material due to its high capture capacity and thermal stability. In this study, the kinetics of carbonation and decarbonation of Li_4SiO_4 was evaluated at atmospheric pressure, isothermal and non-isothermal conditions and in cycling experiments. According to the non-isothermal test, carbonation occurs within 500–715 °C and decarbonation above it. Isothermal tests showed that the reaction rates increased with increasing temperature and at high temperatures it was possible to capture up to 35 wt% CO_2. Kinetics of both carbonation and decarbonation was adequately described by the shrinking core model. The Li_4SiO_4 presented an excellent durability comparing to other materials for CO_2 capture, with an activity decay of 20% after 48 cycles.

1. Introduction

There is a growing interest in the concept of a hydrogen economy, in which H_2 along with electricity can become the main energy carriers. Advantages of this type of energy include the low environmental impact in addition to the application on fuel cell technology aiming the generation of electricity.

Processes to produce hydrogen, as the conventional steam reforming and coal gasification, are operated at a high temperature range (700–900 °C) and have carbon dioxide as one of the products. The removal of CO_2 from the reaction stream can both increase the concentration of the desired products and improve the overall efficiency [1–4].

One of the most promising techniques for CO_2 capture consists in its separation by the reversible reaction with a sorbent. Three

* Corresponding author. Tel.: +55 48 3721 4074.
E-mail addresses: amorim_sm@yahoo.com.br (S.M. Amorim), michedido@gmail.com (M.D. Domenico), tirzhadantas@gmail.com (T.L.P. Dantas), humberto.jose@ufsc.br (H.J. José), regina.moreira@ufsc.br (R.F.P.M. Moreira).

http://dx.doi.org/10.1016/j.cej.2015.07.083
1385-8947/

suitable materials are known to have good capacities for the sorption of CO_2 at high temperatures: CaO-based materials [5–7], hydrotalcites (HT) [2,4,8,9] and lithium based materials [10,11]. Activated carbons and zeolites have been widely used, though the low equilibrium temperature for adsorption (25–150 °C) limits their application.

Calcium oxide (CaO) presents high CO_2 capture capacity in temperatures of 600–700 °C; however, the solid shows poor stability during extended carbonation/decarbonation cycles and requires high energy for complete regeneration (950 °C) [12–14]. Hydrotalcites are more suitable to use in the cyclic process (carbonation/decarbonation) than CaO, but they have lower adsorption capacity [5,15].

The lithium-based ceramics such as lithium oxide (Li_2O), lithium zirconate (Li_2ZrO_3), lithium silicate (Li_4SiO_4), lithium aluminate (Li_5AlO_4), lithium ferrite ($LiFeO_2$) and lithium titanate (Li_4TiO_4) have also been used for CO_2 capture [16]. Li_2O has the highest theoretical capacity (147.3 wt%), but the high reactivity of the solid and corrosion may limit its use [17]. Li_5AlO_4 has also a high capture capacity (70.0 wt%) and wide operating range (200–700 °C), but the sintering during its regeneration can reduce the surface area, and thus, the solid reactivity [17]. Although the Li_2SiO_3 presents a good capture capacity (48.9 wt%) it has a low equilibrium temperature for carbonation (260 °C) [11]. Li_4TiO_4, Li_2ZrO_3 and $LiFeO_2$ present the lower theoretical CO_2 uptakes (31.5, 23.2 and 28.7 wt%, respectively). Finally, the equilibrium temperature of the carbonation reaction for $LiFeO_2$ is relatively low (510 °C) when compared to other ceramics such as Li_2ZrO_3 (715 °C) and Li_4SiO_4 (720 °C) [11].

Among the lithium-based compounds, Li_4SiO_4 appears as a suitable material for CO_2 capture at high temperatures. The reaction of this solid is attributed to the mechanism by which the Li_2O within the crystal structure of Li_4SiO_4 reversibly reacts with CO_2, as given by Eq. (1). The advantages of this solid include a relatively high capture capacity (theoretical value of 36.7 wt%) at temperatures of 450–700 °C, fast kinetics of carbonation/decarbonation, good mechanical properties and also the possibility of use in repeated carbonation/decarbonation cycles [18–20]. Still, there is no enough knowledge related to the regeneration potential of this material [20–22].

$$Li_4SiO_{4(s)} + CO_{2(g)} \leftrightarrow Li_2SiO_{3(s)} + Li_2CO_{3(s)} \quad (1)$$

Understanding the physical and chemical processes that occur during CO_2 capture is extremely important for the proper application of the sorbent, but its regeneration has not been studied in details [16,18,23,24]. The possibility of regenerating the Li_4SiO_4 along with its reuse, make the study of the decarbonation mechanism equally important as the carbonation mechanism and fundamental in the economic point of view. Up to now, it was found that only Qi et al. [23] and Amorim [25] studied the kinetics of both carbonation and decarbonation reactions of Li_4SiO_4. Qi and others [23] tested the fitting of three different models to the experimental data of carbonation: shrinking core model with chemical reaction as the rate-limiting step, double exponential model and Avrami–Erofeev model. The latter presented the best fitting to the results, being later applied to the experimental data of decarbonation.

The Avrami-Erofeev model describes the kinetics of crystallization of solids and, despite presenting a good fit to the experimental data, there is no clear physical interpretation of the model constants [23]. The double exponential model is widely used to describe the carbonation of Li_4SiO_4 [18,21,26,27] since it generally presents good agreement with the kinetic data. In this model, the constants values correspond to the chemical reaction of CO_2 on the particle surface and the chemical reaction controlled by diffusion processes through the layer of products. Although the good fit presented for the carbonation of Li_4SiO_4, there is no other compelling experimental evidence that could validate this model [24].

The shrinking core model has been tested to fit the experimental results for the carbonation reaction of Li_2ZrO_3, considering the internal diffusion in the product layer as the rate-limiting step [28,29]. In this case, limitations by the external diffusion in the gas layer and chemical reaction were excluded. Jimenez and others [30], on the contrary, proposed the fitting of the shrinking core model considering the three rate-limiting steps to the carbonation reaction of Na_2ZrO_3. Ortiz and others [24] applied the same methodology as Jimenez and others [30] to the experimental data of lithium orthosilicate carbonation. Both research groups found excellent results using this approach.

This work presents a kinetic study and modeling of the carbonation and decarbonation reactions of Li_4SiO_4. The regeneration capacity of Li_4SiO_4 for 48 cycles was evaluated in cyclic carbonation/decarbonation experiments in a thermogravimetric analyzer. Isothermal and non-isothermal tests were also carried out and the experimental results were fitted to the shrinking core model considering the three rate-limiting steps: chemical reaction, external diffusion and internal diffusion.

2. Fundamentals of the kinetic model

The mechanism proposed by the shrinking core model assumes the particles as uniform non-porous grains. Initially, the reaction occurs in the grain surface and then the reaction zone moves into the solid leaving a product layer behind. The total radius of the particle remains constant, while the radius of the unreacted core and the layer of products vary over time as a function of conversion.

The approximate solution of the shrinking core model applied in this work is a combination of the resistances that can simultaneously occur in a particle under reaction [31]: CO_2 diffusion in the gas layer surrounding the particle, CO_2 diffusion through the product layer around the unreacted core and chemical reaction on the unreacted core surface. The algebraic solution that relates the conversion as a function of time for a spherical particle is given by:

$$t = \frac{1}{S_m}X + \frac{1}{S_g}[1 - 3(1-X)^{2/3} + 2(1-X)] + \frac{1}{S_r}[1 - (1-X)^{1/3}] \quad (2)$$

where the terms S_m, S_g e S_r represent the resistances to the external mass transfer, product layer diffusion and chemical reaction, respectively, and X is fractional conversion. Carbonation/decarbonation parameters are calculated separately according to the equations presented in Table 1. The model was derived considering carbonation and decarbonation reaction orders of 1 and 0, respectively, with respect to carbon dioxide [24].

In Table 1, b is the stoichiometric coefficient determined by the ratio of moles of Li_4SiO_4 per mol of CO_2 in the carbonation reaction, c is the stoichiometric coefficient determined by the ratio of mols of Li_2CO_3 per mol of CO_2 in the decarbonation reaction, k_g is the

Table 1
Equations used to determine the parameters of the shrinking core model for carbonation/decarbonation reactions of Li_4SiO_4.

Parameters	Equations	
	Carbonation	Decarbonation
S_m	$\frac{3bk_{gc}C_{CO_{2}0}}{r\rho_{Li_4SiO_4}}$	$\frac{3ck_{gd}C_{CO_{2}s}}{r\rho_{Li_2CO_3}}$
S_g	$\frac{6bD_{gc}C_{CO_{2}0}}{r^2\rho_{Li_4SiO_4}}$	$\frac{6cD_{gd}C_{CO_{2}s}}{r^2\rho_{Li_2CO_3}}$
S_r	$\frac{bk_{sc}C_{CO_{2}0}}{r\rho_{Li_4SiO_4}}$	$\frac{bk_{sd}}{r\rho_{Li_4SiO_4}}$
X	$\frac{m_c - m_{c0}}{m_{fc}}$	$\frac{m_{d0} - m_d}{m_{fc}}$

mass transfer coefficient in the gas layer surrounding the particle (cm^3/s), D_g is the CO_2 diffusion coefficient through the product layer (cm^2/s), k_s is the reaction rate constant (cm^3/s), $C_{CO_{2_0}}$ and $C_{CO_{2_s}}$ are the initial concentration of CO_2 in the gas surrounding the particle, respectively, in the carbonation and decarbonation reactions (mol/cm^3), r is the average radius of the particle (cm), $\rho_{Li_4SiO_4}$ is the lithium orthosilicate molar density (mol/cm^3) and $\rho_{Li_2CO_3}$ is the lithium carbonate molar density (mol/cm^3). The conversion is calculated using thermogravimetric data, being m the transient mass, m_0 the initial mass of the reaction, m_{ft} the final mass of the carbonated solid (found by multiplying the theoretical maximum capacity of Li_4SiO_4 and the initial mass of the experiment) and finally m_{fc} is the final mass of the carbonated Li_4SiO_4 (experimentally measured during carbonation stage and prior to decarbonation), all given in mg.

3. Experimental work

3.1. Material

Lithium orthosilicate (Li_4SiO_4) was supplied by *Chemetall* company (Frankfurt, Germany) with purity of 97.5% and is presented as a crystalline powder with a particle diameter up to 350 μm. Gases used in the thermogravimetric tests were nitrogen (purity 99.996 vol%) and industrial carbon dioxide, both supplied by *White Martins* company (Santa Catarina, Brazil).

3.2. Methods

The specific surface area of lithium orthosilicate was calculated using the BET method, being the isotherm of adsorption/desorption obtained in a New 2200E by *Quantachrome*. The particles morphology was determined by scanning electron microscopy (SEM) using a JEOL JSM-6390LV microscope. Finally, crystalline phases of the solid were found by X-ray diffraction (XRD) analysis, conducted in an X'Pert diffractometer by *Philips*, with a *scan* of 0,038/s and Cu Kα radiation.

CO_2 capture tests were carried out in a thermogravimetric analyzer model DTG-60 by *Shimadzu*, at atmospheric pressure. Carbonation of Li_4SiO_4 was done in two sequential stages: (1) pre-treatment and (2) thermal analysis (isothermal and non-isothermal conditions). The pre-treatment was performed in all experiments, at a heating rate of 5 °C/min, from room temperature up to 750 °C, under N_2 atmosphere. The aim of this stage was to eliminate impurities on the solid surface. Non-isothermal analysis was conducted immediately after cooling the solid down to room temperature under N_2 atmosphere, and then by heating the sample at a rate of 10 °C/min up to 1000 °C, in pure CO_2. This test was used to identify the operating temperature range of carbonation/decarbonation of Li_4SiO_4. Isothermal analysis was conducted after cooling the solid down to the carbonation temperature (500–700 °C) under N_2 atmosphere. When the furnace and the sample achieved the desired temperature, the inert gas was replaced by pure CO_2, for both isothermal and non-isothermal procedures.

Decarbonation of Li_4SiO_4 was done in three sequential stages: (1) pre-treatment, (2) isothermal carbonation and (3) isothermal decarbonation. After being pretreated, the solid was carbonated at 700 °C for a period of 60 min, in pure CO_2. Then, the decarbonation temperature was adjusted (550–700 °C) and the CO_2 was replaced by N_2. Experimental data was measured until complete decarbonation of Li_4SiO_4.

Finally, reversibility of the CO_2 capture process was evaluated in an experiment of 48 cycles of carbonation/decarbonation, with each cycle divided into two stages: carbonation in pure CO_2 and decarbonation in pure N_2. Both stages were conducted at 700 °C for 60 min.

N_2 and CO_2 flow rates were set to 200 mL/min during all procedures.

4. Results and discussion

4.1. Characterization

The XRD patterns of the raw, pretreated, carbonated and regenerated lithium orthosilicate samples are shown in Fig. 1. The raw sample presented characteristic peaks of the crystalline phases of Li_4SiO_4 (JCPDS 37-1472), Li_2SiO_3 (JCPDS 83-1517), Li_2CO_3 (JCPDS 83-1554), $LiOH.H_2O$ (JCPDS76-1073) and SiO_2 (JCPDS 82-1568). According to Eqs. (3) and (4), respectively, LiOH and Li_2SiO_3 are products from the reaction of Li_4SiO_4 with steam and Li_2CO_3 and SiO_2 are products from the reaction of Li_4SiO_4 with CO_2. Both reactions can slowly occur at room temperature [10,32].

$$Li_4SiO_{4(s)} + H_2O_{(g)} \leftrightarrow Li_2SiO_{3(s)} + 2LiOH_{(s)} \quad (3)$$

$$Li_4SiO_{4(s)} + CO_{2(g)} \leftrightarrow 2Li_2CO_{3(s)} + SiO_{2(s)} \quad (4)$$

Crystalline phases found for the raw lithium orthosilicate, related to the reactions with steam and carbon dioxide, indicate the importance of the solid treatment prior to the carbonation tests. During the pre-treatment, the solid loses about 12 wt%, resulting in a XRD pattern with the crystalline phases of Li_4SiO_4 and Li_2SiO_3. In this case, the existence of lithium metasilicate can be associated with the synthesis method used to obtain the lithium orthosilicate. Syntheses based on the sol–gel method normally produce residual Li_2SiO_3 [33].

Carbonated Li_4SiO_4 presented characteristic peaks of the crystalline phases of Li_2CO_3 and Li_2SiO_3, which are products from the reaction between the solid and carbon dioxide at temperatures higher than 262 °C, according to Eq. (1) [23]. Finally, the regenerated solid presented the crystalline phases of Li_4SiO_4, Li_2SiO_3 and Li_2CO_3, being the peaks of the last two components of much lower intensity, indicating that the Li_4SiO_4 was almost completely regenerated.

Surface area analysis of the raw Li_4SiO_4 generated an adsorption–desorption isotherm of type II (Fig. A.1 in the Supplementary Material), corresponding to a non-porous or macroporous sorbent. The specific surface area determined by the BET method was approximately 5.6 m^2/g, which is a characteristic value found for other compounds as Li_2ZrO_3, Na_2ZrO_3 and CaO

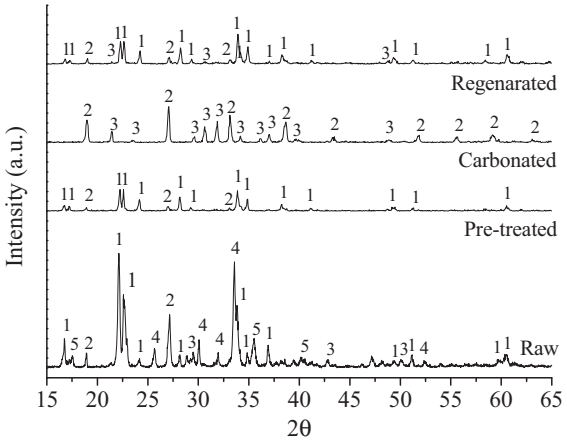

Fig. 1. XRD patterns of the raw, pretreated, carbonated and regenerated Li_4SiO_4. Crystalline phases (1) Li_4SiO_4, (2) Li_2SiO_3, (3) Li_2CO_3, (4) $LiOH{\cdot}H_2O$ and (5) SiO_2 were identified.

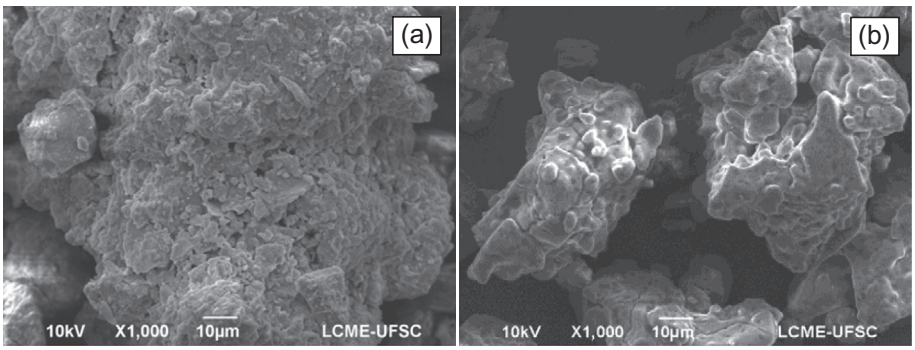

Fig. 2. SEM images of the (a) raw and (b) pretreated Li_4SiO_4.

[24,30,34,35]. The low surface area depending on particle size can be a limiting factor to the carbonation reaction, since the CO_2 has no access to the entire active area of the solid, thus requiring the diffusion of gas through the product layer [21].

The specific surface area of the pretreated Li_4SiO_4 was lower than 1 m^2/g, as observed by Chowdhury and others [22]. The exposure to high temperatures and the elimination of impurities on the solid surface promoted the sintering and decreased the surface area. In this process, there was a removal of existing pores (initial volume 0.06878 cm^3/g) accompanied by a retraction and intense agglomeration of adjacent particles.

The distinct surface areas found for the raw and pretreated samples were also verified by the SEM analysis, as shown in Fig. 2. The raw solid, with higher surface area (Fig. 2a), is basically composed of agglomerates of granular particles, resulting in a rough surface. On the contrary, the pretreated solid (Fig. 2b) presents a very smooth surface, corresponding to the sintering effect, as previously cited.

Thermogravimetric results for the non-isothermal analysis of the pretreated Li_4SiO_4 are shown in Fig. 3. According to the TGA profile, carbonation reaction occurs in the temperature range of 500–715 °C, with a CO_2 uptake of 32 wt% (7.27 mmol CO_2/g Li_4SiO_4), which is close to the maximum theoretical capacity for this solid (36.7 wt%, 8.34 mmol CO_2/g Li_4SiO_4). By the DTA profile it is possible to identify an exothermic peak at 708 °C, associated to the energy released by the carbonation reaction at high temperatures. It indicates that the lithium orthosilicate is a promising material for *in situ* CO_2 capture in processes where the reactions are endothermic, such as steam gasification and methane reforming [10]. Moreover, it is possible to identify an endothermic peak at 718 °C, related to the molten lithium carbonate, which has a relatively low melting point (726 °C) [36].

As shown in the TGA profile, the decarbonation reaction starts at temperatures higher than 715 °C. By the DTA profile it is possible to identify a second endothermic peak at 760 °C, associated to the energy needed to the decarbonation process. Although the Li_4SiO_4 regeneration temperature is high, it is much lower than that required to regenerate CaO, solid widely studied for CO_2 capture (950 °C) [10].

4.2. CO_2 uptake

4.2.1. Cycling tests

The reversibility of CO_2 capture is one of the important aspects to be considered for a good sorbent. In this work, it is highlighted the reversibility of this process using Li_4SiO_4. Conversion results for the cycling analysis are shown in Fig. 4. In the initial cycles, the lithium orthosilicate shows a high CO_2 capture capacity, reaching up to 90 wt% (7.5 mmol CO_2/g Li_4SiO_4) of the stoichiometric value (Eq. (1)) in 60 min at 700 °C. From the eighth cycle, the carbonation capacity decreases, reaching after 48 cycles 74 wt% (6.2 mmol CO_2/g Li_4SiO_4) of the stoichiometric value. It represents an activity decay of 20% of the initial capture capacity.

According to Table 2, HT, Li_2ZrO_3 and Li_4SiO_4 are the sorbents with the lower reduction in capture capacity after cycling tests of carbonation/decarbonation. Even though, HT show low CO_2 capture capacity [3] and the CO_2 capture rate of Li_2ZrO_3 is nearly 30 times smaller than that of Li_4SiO_4 [10]. Then, Li_4SiO_4 seems to be the most suitable sorbent for CO_2 capture at high temperatures.

Carbonation/decarbonation processes promoted changes in the morphology of the solid, as can be seen in the SEM images, shown in Fig. 5. The carbonated Li_4SiO_4 (Fig. 5a) is presented as single particles that after 10 cycles appear to merge (Fig. 5c). After several

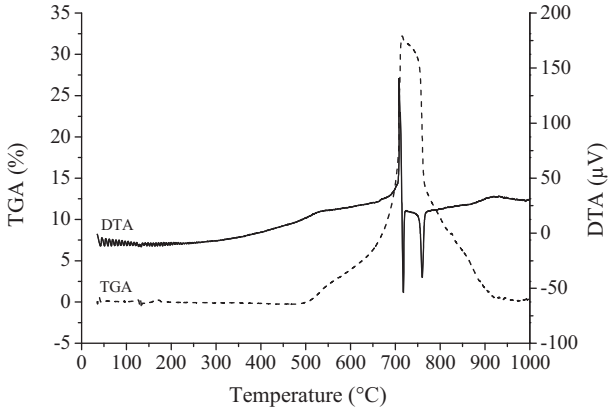

Fig. 3. TGA and DTA profiles as a function of temperature for the non-isothermal analysis of the pretreated Li_4SiO_4 (heating rate of 5 °C/min, pure CO_2).

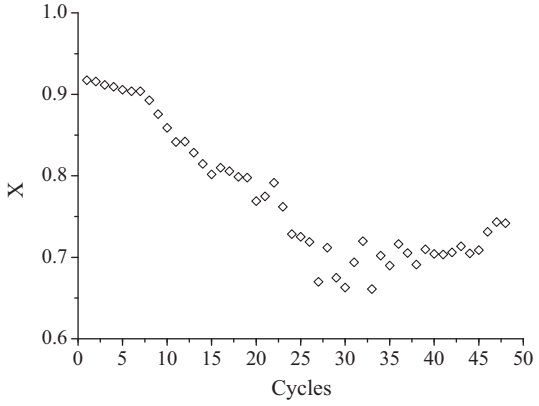

Fig. 4. Conversion as a function of temperature for the cycling experiment of the pretreated Li_4SiO_4 (at 700 °C, carbonation in pure CO_2 and decarbonation in pure N_2).

Table 2
Performance of some materials for high temperature CO_2 capture.

Material	Refs.	Capture			Regeneration		N cycles	Capacity after N cycles, mmol CO_2/g solid
		T, °C	P_{CO_2}, atm	Capacity, mmol CO_2/g solid	T, °C	P_{CO_2}, atm		
CaO	[13]	650	0.15	15.9	850	0	100	3.7
HT*	[3]	400	0.7	0.5	400	0	30	0.4
LiO_2	[16]	28–700	1	27.3	–	–	–	–
Li_2ZrO_3	[37]	575	1	4.1	690	0	11	4.7
Li_4SiO_4	[38]	700	0.5	7.8	700	0	16	6.3
Li_4SiO_4	This work	700	1	7.5	700	0	48	6.2
Li_5AlO_4	[39]	700	1	14.2	750	0	20	1.8

* Hydrotalcites.

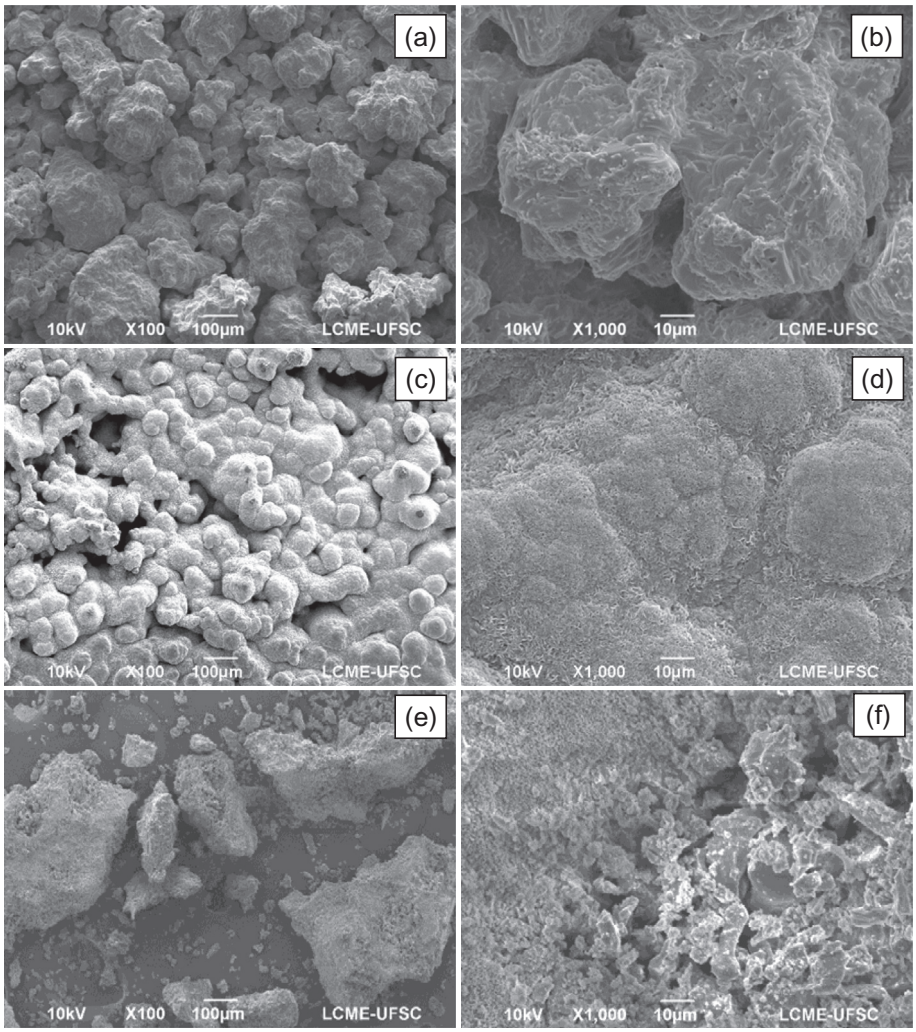

Fig. 5. SEM images of the Li_4SiO_4 (a and b) carbonated, (c and d) after 10 carbonation/decarbonation cycles and (e and f) after 48 carbonation/decarbonation cycles (at 700 °C).

carbonation/decarbonation cycles, the solid surface becomes very rough (Fig. 5d) and the individual outer contours of the particles are less evident. The lithium orthosilicate submitted to 48 cycles as well as the other carbonated samples, formed agglomerates of sintered particles. In this case, the exposure to high temperatures for a long period of time conducted to a very difficult removal of the samples from the support, breaking them as can be seen in Fig. 5e. Nevertheless, it can be seen in Fig. 5e that the individual outer contours no longer exist and, in Fig. 5d and f, that the solid surface remains very rough.

It is well-known that the lithium carbonate may cause reconstruction and sintering during carbonation/decarbonation processes, slowing the CO_2 diffusion and decreasing the capture capacity [12] (Fig. 4). Although the cycling tests were conducted at lower temperatures (700 °C) than that of lithium carbonate melting point (726 °C), it is a fact that the sintering phenomenon promotes the particle agglomeration in temperatures close to the melting point [40].

4.2.2. Kinetics of the carbonation reaction

Thermogravimetric results for the isothermal carbonation analyzes are shown in Fig. 6. The mechanism for CO_2 capture in lithium compounds appears to occur in two steps. First, there is the reaction of CO_2 on the particle surface, until the complete formation of the product layer, composed by lithium carbonate and lithium metasilicate. In the second step, the reaction becomes

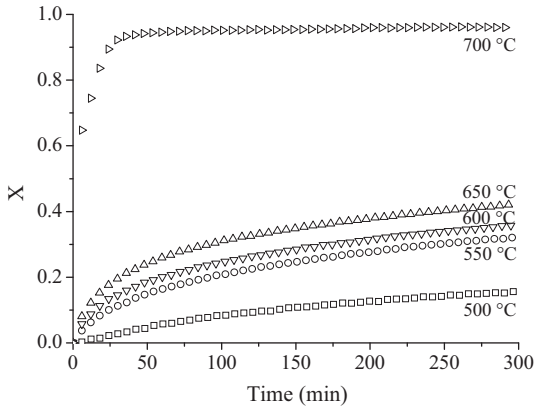

Fig. 6. Conversion vs. time for the isothermal carbonation analysis of the pretreated Li_4SiO_4 (pure CO_2).

controlled by diffusive processes, either by the lithium diffusion in the reaction products or the CO_2 diffusion in the produced layer of Li_2CO_3 [16,23]. Fig. 6 shows that the carbonation kinetics is very fast in the beginning due to the CO_2 reaction on the exposed surface of Li_4SiO_4. As the reaction progresses, there is a decrease in the reaction rate due to diffusive limitations.

According to the kinetic results, it is reasonable to assume that the initial linear fraction of the curves corresponds to the carbonation reaction. Thus, the overall reaction rates for each temperature were estimated by the linear curve slope $\Delta X/\Delta t$, at times close to zero, according to the methodology presented by Jiménez and others [30]. The kinetic expression for the carbon dioxide consumption rate is given by,

$$-r_A = \frac{dX}{dt} = k y_{CO_2}^n \tag{5}$$

where k is the reaction rate constant (1/s), y_{CO_2} is the molar fraction of CO_2 in the atmosphere surrounding the particle and n is the reaction order with respect to CO_2. The Arrhenius equation is used to correlate the rate constant to the temperature and to the activation energy, according to the following kinetic expression,

$$-r_A = k_0 \exp\left(\frac{-Ea}{RT}\right) y_{CO_2}^n \tag{6}$$

where k_0 is the frequency factor (1/s), Ea is the activation energy (kcal/mol), R is the constant of gases (1.987×10^{-3} kcal/mol K) and T is the reaction temperature (K). In this case, n is considered as equal to 1 for the carbonation reaction [24]. With the initial rate values, a plot of $\ln(-r_A)$ vs. $1/T$ results in the expression given by Eq. (7), with R^2 of 0.9997.

$$\ln[-r_A] = -\frac{(20616.94 \pm 2.15)}{T} + (19.65 \pm 0.00) \tag{7}$$

The apparent activation energy was 40.97 ± 0.00 kcal/mol, which is a higher value than that found by Ortiz and others [24], of 22.5 kcal/mol. A possible explanation for this result could be the presence of impurities (Li_2SiO_3) in the sorbent used in this work, which were not present in the pure Li_4SiO_4 used by Ortiz et al. [23]. Other factors could be also affecting, like the porous structure of the different samples and the treatment conditions prior to the CO_2 capture process that can reduce the surface area due to the sintering effect.

The shrinking core model was fitted to the experimental data using the algebraic solution given by Eq. (2). The X vs. t curves for the carbonation reaction (Fig. 6) and the resistance coefficients S_m, S_g e S_r were determined for each temperature, by means of a non-linear regression using *Origin*®. The resistance to the external mass transfer, S_m, appeared to be negligible when compared to the resistances S_g e S_r, thus not limiting the carbonation process. Once different gas flow rates were tested, it was possible to minimize the effects of the external mass transfer.

S_g represents the resistance contribution to the product layer diffusion and S_r is related to the surface chemical reaction [24]. The resistance coefficients that best fitted the experimental data, along with the determining coefficient values (R^2) are presented in Table 3. It was observed that S_r is higher than S_g, but the relation S_g/S_r could be affected by the particle size, since the product layer diffusion becomes more significant as the particle size increases. In fact, by using very small particles of Li_4SiO_4 (7 μm), López Ortiz et al. [24] found that $S_g > S_r$, indicating that the surface chemical reaction exhibits most of the resistance to the reaction.

In addition, in Table 3, are presented the calculated values for the CO_2 diffusion coefficient through the gas layer (D_g) and the reaction rate constant (k_s). The following parameters were used to estimate D_g and k_s: stoichiometric coefficient of Eq. (1) ($b = 1$), $C_{CO_{20}} = 4.49 \times 10^{-5}$ mol/cm^3, $\rho_{Li_4SiO_4} = 0.020$ mol/cm^3 and $r = 0.0175$ cm (value provided by the supplier).

In the lowest temperature range, where the process is limited by the mass transfer, the shrinking core model presented a good fitting to the experimental data. However, for temperatures higher than 650 °C, the model did not describe the behavior of the solid under carbonation, as can be noted by the determination coefficients in Table 3. This result is consistent with the explanation given by the model, which considers the formation of an external

Table 3
Resistance coefficients S_g and S_r, calculated values of D_g and k_s and determining coefficients R^2.

T, °C	S_g, s^{-1}	S_r, s^{-1}	D_{gc}, cm^2/s	k_{sc}, cm/s	R^2
500	$7.14 \times 10^{-7} \pm 1.23 \times 10^{-9}$	$1.04 \times 10^{-5} \pm 3.44 \times 10^{-8}$	$1.63 \times 10^{-8} \pm 2.81 \times 10^{-11}$	$8.14 \times 10^{-5} \pm 2.68 \times 10^{-7}$	0.9964
550	$2.42 \times 10^{-6} \pm 5.51 \times 10^{-9}$	$3.32 \times 10^{-4} \pm 2.92 \times 10^{-5}$	$5.50 \times 10^{-8} \pm 1.25 \times 10^{-10}$	$2.59 \times 10^{-3} \pm 2.27 \times 10^{-4}$	0.9884
600	$3.21 \times 10^{-6} \pm 1.24 \times 10^{-8}$	$5.14 \times 10^{-4} \pm 1.01 \times 10^{-4}$	$7.30 \times 10^{-8} \pm 2.82 \times 10^{-10}$	$4.01 \times 10^{-3} \pm 7.90 \times 10^{-4}$	0.9706
650	$4.85 \times 10^{-6} \pm 3.10 \times 10^{-8}$	$2.42 \times 10^{-3} \pm 2.95 \times 10^{-4}$	$1.10 \times 10^{-7} \pm 7.06 \times 10^{-10}$	$1.89 \times 10^{-2} \pm 2.30 \times 10^{-3}$	0.9348
700	$2.69 \times 10^{-4} \pm 1.34 \times 10^{-5}$	$1.74 \times 10^{-2} \pm 5.89 \times 10^{-2}$	$6.12 \times 10^{-6} \pm 3.05 \times 10^{-7}$	$1.36 \times 10^{-1} \pm 4.60 \times 10^{-1}$	0.7753

Table 4
Arrhenius relation for k_s e D_g.

	Chemical reaction	Diffusion
Equation	$\ln[k_{sc}] = -\frac{(29317.29 \pm 483.24)}{T} + (28.50 \pm 0.62)$	$\ln[D_{gc}] = -\frac{(10835.41 \pm 21.01)}{T} - (3.83 \pm 0.03)$
R^2	0.9186	0.8712
Ea, kcal/mol	58.25 ± 0.96	21.53 ± 0.04

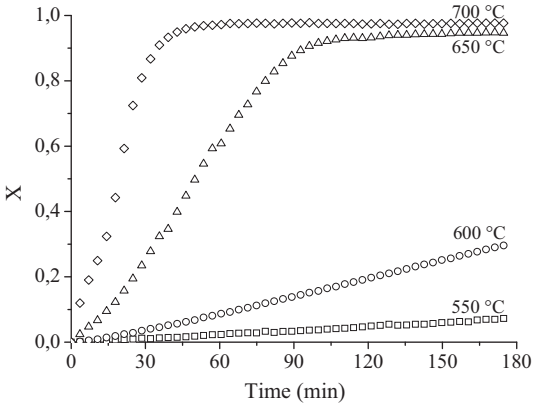

Fig. 7. Conversion vs. time for the isothermal decarbonation analysis of the carbonated Li_4SiO_4 (pure N_2).

product layer around the unreacted core of the solid, thus limiting the chemical reaction. An increment in temperature accelerates the diffusion through the solid layer, increasing the overall rate of reaction [16]. It occurs specially close to the melting point of the lithium carbonate due to the sintering effect.

It can be noted in Table 3 that the D_g values have the same order of magnitude as the diffusion coefficients of gases in solids [41]. Also, an increment in temperature increases both the diffusion coefficient and the reaction rate constant, being the latter most influenced. The gradual increase of D_g is observed up to 650 °C and at 700 °C there is a sharply increase, again explained by the incipient melting of the solid caused by proximity to the lithium carbonate melting point (718 °C).

The dependence of k_s and D_g on temperature was determined by the Arrhenius relation, and the diffusion and intrinsic activation energies were obtained as presented in Table 4. Both the diffusion and intrinsic activation energies were calculated disregarding the temperature of 700 °C due to the small value of R^2 and the large standard deviation calculated for the fitting of S_r (Table 3).

The intrinsic activation energy was 58.25 ± 0.96 kcal/mol, which is only three times higher than that found for the diffusional activation energy, of 21.53 ± 0.04 kcal/mol. It is important to notice that the apparent activation energy (40.97 ± 0.00 kcal/mol) is half of the total activation energy (79.78 ± 1.02 kcal/mol), indicating the influence of both resistances in the CO_2 capture process [41].

The comparison between the experimental data and the shrinking core model fitting of the Li_4SiO_4 carbonation reaction are shown in the Supplementary Material (Fig. A.2).

4.2.3. Kinetics of the decarbonation reaction

Thermogravimetric results for the isothermal decarbonation analyzes are shown in Fig. 7. The isotherms found in this work are very similar to that reported by Qi and others [23] for the decarbonation process. Also, it can be noted that the carbonation and decarbonation isotherms present a distinct behavior, once the diffusion limiting stage does not seem to appear in the decarbonation curves. This could be related either by the absence of diffusive limitations as by the slow rate of the chemical reaction.

Since the decarbonation is a solid–solid reaction, as given by Eq. (8), it is evident that it is slower than the carbonation, which is a gas–solid reaction.

$$Li_2CO_{3_{(s)}} + Li_2SiO_{3_{(s)}} \leftrightarrow Li_4SiO_{4_{(s)}} + CO_{2_{(g)}} \quad (8)$$

The overall reaction rates for each temperature were estimated by the linear curve slope $\Delta X/\Delta t$, being this linear fraction associated to the chemical reaction of decarbonation. The kinetic expression for the carbon dioxide production rate is given by Eq. (5), with a plus sign. It was assumed a decarbonation reaction order of zero with respect to CO_2, which was confirmed by the experimental data. The CO_2 concentration at the gas phase is negligible since a pure N_2 was used to purge the system. The apparent activation energy was determined by fitting the linear model of Eq. (6) to the experimental data. Eq. (9) was obtained with R^2 of 0.9885.

$$\ln[r_A] = -\frac{(28493.64 \pm 0.04)}{T} + (26.38 \pm 0.00) \quad (9)$$

The apparent activation energy for the decarbonation was 56.62 ± 0.00 kcal/mol, which is a higher value than that found for the carbonation reaction. The algebraic solution of the shrinking core model and the X vs. t curves for decarbonation were used to determine the resistance coefficients S_m, S_g e S_r. The resistances to the external and internal mass transfer, S_m and S_g, respectively, appeared to be negligible when compared to the resistance S_r, thus not limiting the decarbonation process.

The resistance coefficients S_r, the determining coefficient values (R^2) and the reaction rate constants (k_{sd}) are presented in Table 5. As noted for the carbonation process, the reaction rate constant is strongly influenced by the temperature. Moreover, according to R^2 values, the shrinking core model presented a good fitting to the experimental data, in the tested temperature range.

Table 5
Resistance coefficients S_r, calculated values of k_s and determining coefficients R^2.

T, °C	S_r, s^{-1}	k_{sd}, mol/cm^2 s	R^2
550	$2.24 \times 10^{-6} \pm 9.55 \times 10^{-10}$	$7.87 \times 10^{-10} \pm 3.35 \times 10^{-13}$	0.9924
600	$1.02 \times 10^{-5} \pm 6.77 \times 10^{-9}$	$3.57 \times 10^{-9} \pm 2.37 \times 10^{-12}$	0.9786
650	$8.24 \times 10^{-5} \pm 1.01 \times 10^{-5}$	$2{,}89 \times 10^{-8} \pm 3.55 \times 10^{-9}$	0.9485
700	$2.27 \times 10^{-4} \pm 2.63 \times 10^{-5}$	$7.97 \times 10^{-8} \pm 9.23 \times 10^{-9}$	0.9540

The dependence of k_s on temperature was determined by the Arrhenius relation and the linear Eq. (10) was obtained with R^2 of 0.9999.

$$\ln[k_s] = -\frac{(21726.38 \pm 11.35)}{T} + (5.43 \pm 0.01) \quad (10)$$

The intrinsic activation energy for the decarbonation was 43.17 ± 0.02 kcal/mol, which is lower than the calculated apparent activation energy. As previously mentioned, Qi and others [23] applied the Avrami-Erofeev model to the experimental data of the decarbonation of a commercial Li_4SiO_4. The authors found that the chemical reaction step controlled the process, with an activation energy of 85 kcal/mol.

The comparison between the experimental data and the shrinking core model fitting of the Li_4SiO_4 decarbonation reaction are shown in the Supplementary Material (Fig. A.3).

5. Conclusions

In this study, the regeneration of lithium orthosilicate (Li_4SiO_4) was evaluated in carbonation/decarbonation experiments. It was observed that the CO_2 capture capacity decays after 20 cycles and remains nearly constant up to 48 reaction cycles of carbonation/decarbonation. The kinetics of carbonation and decarbonation reactions of Li_4SiO_4 was well fitted to the shrinking core model. The intrinsic and diffusional activation energies for the carbonation were 58.25 and 21.53 kcal/mol, respectively, and the intrinsic activation energy for the decarbonation was 43.17 kcal/mol. The wide temperature range for carbonation (500–715 °C), the high capture capacity (35 wt%), the regeneration at lower temperatures (715 °C) and the advantage of use in repeated cycles, make this solid potentially competitive when compared to other materials used for CO_2 capture at high temperatures.

Notation

b	stoichiometric coefficient of reaction (1)
c	stoichiometric coefficient of reaction (8)
$C_{CO_{2_0}}$	initial concentration of CO_2 around the particle for the carbonation, mol/cm^3
$C_{CO_{2_s}}$	initial concentration of CO_2 around the particle for the decarbonation, mol/cm^3
D_{gc}	CO_2 diffusion coefficient through the product layer for the carbonation, cm^2/s
D_{gd}	CO_2 diffusion coefficient through the product layer for the decarbonation, cm^2/s
Ea	activation energy, kcal/mol
k	reaction rate constant, 1/s
k_{gc}	mass transfer coefficient in the gas layer around the particle for the carbonation, cm^3/s
k_{gd}	mass transfer coefficient in the gas layer around the particle for the decarbonation, cm^3/s
k_{sc}	chemical reaction rate constant for the carbonation, cm^3/s
k_{sd}	chemical reaction rate constant for the decarbonation, cm^3/s
k_0	frequency factor, 1/s
m_c	transient mass during the carbonation, mg
m_{c0}	initial mass of the carbonation, mg
m_d	transient mass during the decarbonation, mg
m_{d0}	initial mass of the decarbonation, mg
m_{fc}	final mass of the carbonated solid, mg
m_{ft}	theoretical final mass of the carbonated solid, mg
n	reaction order
r	average radius of the solid particle, cm
r_A	reaction rate, 1/s
R	constant of gases, kcal/mol K
S_g	resistance to the product layer diffusion, 1/s
S_m	resistance to the external mass transfer, 1/s
S_r	resistance to the chemical reaction, 1/s
t	time, s
T	temperature, K
X	fractional conversion
y_{CO_2}	molar fraction of CO_2 around the particle
Greek symbols	
$\rho_{Li_2CO_3}$	lithium carbonate molar density, mol/cm^3
$\rho_{Li_4SiO_4}$	lithium orthosilicate molar density, mol/cm^3

Acknowledgments

This research was supported by the Coordination for the Improvement of Higher Education Personnel (CAPES-Brazil) and National Counsel of Technological and Scientific Development (CNPq-Brazil). The authors would like to thank the LCME-UFSC for the technical support during electron microscopy work. The authors also wish to thank the PhD Vanessa Zanon Baldissarelli for her collaboration in the specific surface area analyzes of the samples.

Appendix A. Supplementary data

Supplementary data associated with this article can be found, in the online version, at http://dx.doi.org/10.1016/j.cej.2015.07.083.

References

[1] M.H. Halabi, M.H.J.M. de Croon, J. van der Schaaf, P.D. Cobden, J.C. Schouten, Reactor modeling of sorption-enhanced autothermal reforming of methane. Part I. Performance study of hydrotalcite and lithium zirconate-based processes, Chem. Eng. J. 168 (2011) 872–882.
[2] S.G. Mayorga, J.R. Hufton, T.R. Gaffney, Sorption Enhanced Reaction Process for Production of Hydrogen. Phase I Final Report, Washington, DC, 1997.
[3] J.R. Hufton, S. Mayorga, S. Sircar, Sorption-enhanced reaction process for hydrogen production, AIChE J. 45 (1999) 248–256.
[4] E.L.G. Oliveira, C.A. Grande, A.E. Rodrigues, Effect of catalyst activity in SMR-SERP for hydrogen production: commercial vs. large-pore catalyst, Chem. Eng. Sci. 66 (2011) 342–354.
[5] N. Chanburanasiri, A.M. Ribeiro, A.E. Rodrigues, A. Arpornwichanop, N. Laosiripojana, P. Praserthdam, et al., Hydrogen production via sorption enhanced steam methane reforming process using Ni/CaO multifunctional catalyst, Ind. Eng. Chem. Res. 50 (2011) 13662–13671.
[6] A. Lopez, D.P. Ortiz, Harrison, hydrogen production using sorption-enhanced reaction, Ind. Eng. Chem. Res. 40 (2001) 5102–5109.
[7] E.L.G. Oliveira, C.A. Grande, A.E. Rodrigues, CO_2 sorption on hydrotalcite and alkali-modified (K and Cs) hydrotalcites at high temperatures, Sep. Purif. Technol. 62 (2008) 137–147.
[8] A.F. Cunha, Y.J. Wu, F.A. Díaz Alvarado, J.C. Santos, P.D. Vaidya, A.E. Rodrigues, Steam reforming of ethanol on a Ni/Al_2O_3 catalyst coupled with a hydrotalcite-like sorbent in a multilayer pattern for CO_2 uptake, Can. J. Chem. Eng. 90 (2012) 1514–1526.
[9] Y.-J. Wu, P. Li, J.-G. Yu, A.F. Cunha, A.E. Rodrigues, K-promoted hydrotalcites for CO_2 capture in sorption enhanced reactions, Chem. Eng. Technol. 36 (2013) 567–574.
[10] M. Kato, K. Nakagawa, K. Essaki, Y. Maezawa, S. Takeda, R. Kogo, et al., Novel CO_2 absorbents using lithium-containing oxide, Int. J. Appl. Ceram. Technol. 2 (2005) 467–475.
[11] H. Nakagawa, K. Kato, M. Yoshikawa, S. Essaki, K. Uemoto, A novel CO_2 absorbent using lithium-containing oxides, Proc. 2nd Annu. Conf. Carbon Sequestration, Alexandria, 2003, p. 6.
[12] X.S. Yin, M.A. Song, Q.H. Zhang, J.G. Yu, High-temperature CO_2 capture on $Li_6Zr_2O_7$: experimental and modeling studies, Ind. Eng. Chem. Res. 49 (2010) 6593–6598.
[13] N.H. Florin, A.T. Harris, Reactivity of CaO derived from nano-sized $CaCO_3$ particles through multiple CO_2 capture-and-release cycles, Chem. Eng. Sci. 64 (2009) 187–191.
[14] J.C. Abanades, The maximum capture efficiency of CO_2 using a carbonation/calcination cycle of CaO/$CaCO_3$, Chem. Eng. J. 90 (2002) 303–306.
[15] Z. Yong, V. Mata, A. Rodrigues, Adsorption of carbon dioxide at high temperature – a review, Sep. Purif. Technol. 26 (2002) 195–205.
[16] J. Ortiz-Landeros, T. Ávalos-Rendón, C. Gómez-Yáñez, H. Pfeiffer, Analysis and perspectives concerning CO_2 chemisorption on lithium ceramics using thermal analysis, J. Therm. Anal. Calorim. 108 (2012) 647–655.
[17] T. Ávalos-Rendón, J. Casa-Madrid, H. Pfeiffer, Thermochemical capture of carbon dioxide on lithium aluminates ($LiAlO_2$ and Li_5AlO_4): a new option for the CO_2 absorption, J. Phys. Chem. A 113 (2009) 6919–6923.
[18] M.J. Venegas, E. Fregoso-Israel, R. Escamilla, H. Pfeiffer, Kinetic and reaction mechanism of CO_2 sorption on Li_4SiO_4: study of the particle size effect, Ind. Eng. Chem. Res. 46 (2007) 2407–2412.
[19] M. Seggiani, M. Puccini, S. Vitolo, High-temperature and low concentration CO_2 sorption on Li_4SiO_4 based sorbents: Study of the used silica and doping method effects, Int. J. Greenh. Gas Control. 5 (2011) 741–748.
[20] K. Wang, X. Guo, P. Zhao, F. Wang, C. Zheng, High temperature capture of CO_2 on lithium-based sorbents from rice husk ash, J. Hazard. Mater. 189 (2011) 301–307.
[21] I.C. Romero-Ibarra, J. Ortiz-Landeros, H. Pfeiffer, Microstructural and CO_2 chemisorption analyses of Li_4SiO_4: effect of surface modification by the ball milling process, Thermochim. Acta 567 (2013) 118–124.
[22] M.B.I. Chowdhury, M.R. Quddus, H.I. DeLasa, CO_2 capture with a novel solid fluidizable sorbent: thermodynamics and temperature programmed carbonation–decarbonation, Chem. Eng. J. 232 (2013) 139–148.
[23] Z. Qi, Z. Daying, H. Yang, L. Zibin, Analysis of CO_2 sorption/desorption kinetic behaviours and reaction mechanisms on Li_4SiO_4, AIChE J. 59 (2012) 901–911.
[24] A. López Ortiz, M.A. Escobedo Bretado, V. Guzmán Velderrain, M. Meléndez Zaragoza, J. Salinas Gutiérrez, D. Lardizábal Gutiérrez, et al., Experimental and modeling kinetic study of the CO_2 absorption by Li_4SiO_4, Int. J. Hydrogen Energy 39 (2014) 16656–16666.
[25] S.M. de Amorim, CO_2 capture at high temperatures through the carbonation reaction of lithium orthosilicate (Li_4SiO_4), Federal University of Santa Catarina, 2013.
[26] R. Rodríguez-Mosqueda, H. Pfeiffer, Thermokinetic analysis of the CO_2 chemisorption on Li_4SiO_4 by using different gas flow rates and particle sizes, J. Phys. Chem. A 114 (2010) 4535–4541.
[27] K. Wang, P. Zhao, X. Guo, Y. Li, D. Han, Y. Chao, Enhancement of reactivity in Li_4SiO_4-based sorbents from the nano-sized rice husk ash for high-temperature CO_2 capture, Energy Convers. Manage. 81 (2014) 447–454.
[28] J. Ida, R. Xiong, Y.S. Lin, Synthesis and CO_2 sorption properties of pure and modified lithium zirconate, Sep. Purif. Technol. 36 (2004) 41–51.
[29] G. Pannocchia, M. Puccini, M. Seggiani, S. Vitolo, Experimental and modeling studies on high-temperature capture of CO_2 using lithium zirconate based sorbents, Ind. Eng. Chem. Res. 46 (2007) 6696–6706.
[30] D. Barraza Jiménez, M.A. Escobedo Bretado, D. Lardizábal Gutiérrez, J.M. Salinas Gutiérrez, A. López Ortiz, V. Collins-Martínez, Kinetic study and modeling of the high temperature CO_2 capture by Na_2ZrO_3 solid absorbent, Int. J. Hydrogen Energy 38 (2013) 2557–2564.

[31] O. Levenspiel, Chemical Reaction Engineering, John Wiley & Sons, New York, 1999.
[32] J. Ortiz-Landeros, L. Martínez-dlCruz, C. Gómez-Yáñez, H. Pfeiffer, Towards understanding the thermoanalysis of water sorption on lithium orthosilicate (Li_4SiO_4), Thermochim. Acta 515 (2011) 73–78.
[33] H. Pfeiffer, P. Bosch, S. Bulbulian, Synthesis of lithium silicates, J. Nucl. Mater. 257 (1998) 309–317.
[34] R. Xiong, J. Ida, Y.S. Lin, Kinetics of carbon dioxide sorption on potassium-doped lithium zirconate, Chem. Eng. Sci. 58 (2003) 4377–4385.
[35] V. Nikulshina, M.E. Gálvez, A. Steinfeld, Kinetic analysis of the carbonation reactions for the capture of CO_2 from air via the $Ca(OH)_2$–$CaCO_3$–CaO solar thermochemical cycle, Chem. Eng. J. 129 (2007) 75–83.
[36] D.L. Perry, Handbook of Inorganic Compounds, second ed., Taylor & Francis, 2011.
[37] H.R. Radfarnia, M.C. Iliuta, Surfactant-template/ultrasound-assisted method for the preparation of porous nanoparticle lithium zirconate, Ind. Eng. Chem. Res. 50 (2011) 9295–9305.
[38] S. Shan, Q. Jia, L. Jiang, Q. Li, Y. Wang, J. Peng, Novel Li_4SiO_4-based sorbents from diatomite for high temperature CO_2 capture, Ceram. Int. 39 (2013) 5437–5441.
[39] T. Ávalos-Rendón, V.H. Lara, H. Pfeiffer, CO_2 chemisorption and cyclability analyses of lithium aluminate polymorphs (α- and β-Li_5AlO_4), Ind. Eng. Chem. Res. 51 (2012) 2622–2630.
[40] S. Sōmiya, F. Aldinger, N. Claussen, R.M. Spriggs, K. Uchino, K. Koumoto, et al., Handbook of Advanced Ceramics, Elsevier, 2003. pp. 187–264.
[41] H.S. Fogler, Elements of Chemical Reaction Engineering, Prentice Hall, New Jersey, 1992.